Applied Catalysis B: Environmental 154–155 (2014) 246–251

Contents lists available at ScienceDirect

Applied Catalysis B: Environmental

journal homepage: www.elsevier.com/locate/apcatb

Shape-controlled activation of peroxymonosulfate by single crystal α-Mn_2O_3 for catalytic phenol degradation in aqueous solution

Edy Saputra[a,b], Syaifullah Muhammad[a,c], Hongqi Sun[a], Ha-Ming Ang[a], Moses O. Tadé[a], Shaobin Wang[a,*]

[a] Department of Chemical Engineering and CRC for Contamination Assessment and Remediation of the Environment (CRC CARE), Curtin University, GPO Box U1987, Perth, WA 6845, Australia
[b] Department of Chemical Engineering, Riau University, Pekanbaru 28293, Indonesia
[c] Department of Chemical Engineering, Syiah Kuala University, Banda Aceh, Indonesia

ARTICLE INFO

Article history:
Received 2 December 2013
Received in revised form 12 February 2014
Accepted 15 February 2014
Available online 24 February 2014

Keywords:
Mn_2O_3
Shape-control
Phenol degradation
Water treatment
Sulfate radical

ABSTRACT

Shape selective reaction on crystallite particles is an important issue in catalytic reactions. In this investigation, Mn_2O_3 crystals with different shapes were prepared and tested in activation of peroxymonosulfate to produce sulfate radicals for degradation of aqueous phenol. The Mn_2O_3 shaped in cube, octahedra and truncated octahedra showed different activities in phenol degradation. Cubic Mn_2O_3 presented the highest activity among the three catalysts with an order of Mn_2O_3-cubic > Mn_2O_3-octahedra > Mn_2O_3-truncated, attributed to high surface area and surface atoms arrangement. In addition, kinetic studies showed that phenol degradation on Mn_2O_3-cubic follows first-order kinetics with activation energy of 61.2 kJ/mol.

1. Introduction

Worldwide attention to the problem of clean water is increasing day by day because of the increasing need of clean water with the expansion in population and economy [1]. However, the problem is not due to depletion of fresh water, but the damage caused by industrial and human activities. In order to make significant improvement in water supply, the research in water treatment has been rapidly growing. In the last decades, advanced oxidation processes (AOPs) provide a very promising technology for degradation of a wide range of organic compounds in aqueous media. Nowadays, most AOPs are based on the generation of reactive species (hydroxyl radicals, •OH) that have a higher oxidation potential and would be able to oxidize almost all organic compounds [2]. More recently, sulfate radicals ($SO4^{\bullet-}$) have been attracting extensive interest and suggested to be a substitution to the hydroxyl radicals due to their higher oxidation potential (E^0) of HSO_5^-/HSO_4^- = 1.82 V than that of hydrogen peroxide (E^0) of H_2O_2/H_2O = 1.76 V [3].

In the past few years, several investigations have suggested that Co^{2+}/peroxymonosulfate (Oxone®, HSO_5^-) is an effective route for generation of sulfate radicals [4–6]. However, utilizing Co^{2+} ions as catalysts to activate Oxone® will raise an issue of toxicity of cobalt ions in water, because cobalt is a heavy metal which can cause diseases to animals and human beings. Therefore, alternative metals such as iron (Fe^0 or Fe^{2+}) have been proposed [7–9], however, Fe exhibited much lower activity. Anipsitakis and Dionysiou [4] studied several metal ions, Fe^{2+}, Fe^{3+}, Co^{2+}, Mn^{2+}, Ni^{2+}, Ru^{3+}, Ce^{3+}, and Ag^+ for the activation of peroxymonosulfate, hydrogen peroxide, and peroxydisulfate for 2,4-dicholorophenol degradation. They found that the conjunction of Ce^{3+}, Mn^{2+}, and Ni^{2+} ions with peroxymonosulfate (Oxone®) also showed the generation of sulfate radicals. We have compared Co_3O_4, Fe_3O_4 and Mn_3O_4 catalysts in peroxymonosulfate activation and found that Mn_3O_4 is a better catalyst than the other two [10].

As it is well known, manganese oxides, such as MnO, MnO_2, Mn_2O_3 and Mn_3O_4 have a redox cycle between 2+ and 4+ oxidation states, providing a good redox reaction of Mn^{2+}/Mn^{3+} or Mn^{3+}/Mn^{4+}, and oxygen mobility in the oxide lattice. This property enhances the performance of manganese oxide catalysts used in AOPs for wastewater treatment. Saputra et al. [11,12] studied several α-MnO_2 catalysts for heterogeneous activation of Oxone® to generate sulfate radicals ($SO_5^{\bullet-}$, and $SO_4^{\bullet-}$) for phenol degradation. They found that MnO_2 exhibited varying activities in activation of peroxymonosulfate to produce sulfate radicals for phenol degradation depending on structure and morphology.

* Corresponding author. Tel.: +61 892663776.
E-mail addresses: Shaobin.wang@curtin.edu.au, wangshao@vesta.curtin.edu.au (S. Wang).

http://dx.doi.org/10.1016/j.apcatb.2014.02.026
0926-3373/

Crystalline structure of MnO_2 is more important than porous structure in influencing the activity of catalyst. They also conducted a study on the heterogeneous catalytic degradation of phenol in aqueous solution on a series of manganese oxides [13]. The work showed that α-Mn_2O_3 is the best catalyst, with the sequence of catalytic activity as $Mn_2O_3 > MnO > Mn_3O_4 > MnO{\cdot}Mn_2O_3$, which was correlated with oxidation state and oxygen mobility on the catalysts.

Recently, shape- or facet-controlled synthesis of catalytic nanoparticles is of paramount importance for both reactive and selective catalysis [14–18]. It is believed that designing and fabricating high-reactive facets of metals or metal oxides would significantly enhance catalytic performance. However, few investigations have been reported on shape controlled catalysis on manganese oxides [19–22]. In particular, no such investigation has been reported in different shapes of metal oxide crystals for heterogeneous activation of peroxymonosulfate. In this research, we investigate for the first time the performance of α-Mn_2O_3 crystals with varying shapes such as cube, octahedra and truncated octahedra in heterogeneous generation of sulfate radicals for chemical mineralization of phenol in solution. The physicochemical properties, catalytic performance, and regeneration of used catalysts were also reported.

2. Experimental

2.1. Material synthesis

Three α-Mn_2O_3 catalysts with different shapes were synthesized by solvothermal and hydrothermal methods reported by Li et al. [23] and Lei et al. [24]. α-Mn_2O_3 in octahedral shape was obtained using ethanol as a solvent. Typically, 4 mmol of $Mn(NO_3)_2{\cdot}4H_2O$ was dissolved in 13 mL of ethanol and then put into distilled water at room temperature to form a homogeneous solution, which was later transferred into a 23 mL Teflon-lined autoclave. The autoclave was sealed and maintained at 120 °C for 10 h, and was then cooled down to room temperature naturally. The solid product, α-Mn_2O_3 octahedra, was filtered, washed with distilled water and dried in air at 100 °C overnight. This sample was referred as α-Mn_2O_3-octahedra. The second sample (α-Mn_2O_3 truncated-octahedra) was obtained by the similar method but using 2-butanol as a solvent, which was referred as α-Mn_2O_3-truncate. Another α-Mn_2O_3 was obtained by a two-step method [24]. Firstly, $MnCO_3$ was synthesized by a hydrothermal method and then was calcined to form Mn_2O_3. Typically, $KMnO_4$ (3 mmol) and an equal amount of glucose were put into distilled water at room temperature to form a homogeneous solution, and then transferred into a 45 mL Teflon-lined autoclave. The autoclave was sealed and maintained at 150 °C for 10 h, and was then cooled down to room temperature naturally. The resulted solid product ($MnCO_3$) was filtered, washed with distilled water and dried in air at 100 °C overnight. Finally, α-Mn_2O_3 cube-like catalyst was obtained by calcination of $MnCO_3$ at 500 °C under air for 2 h. This sample was referred as α-Mn_2O_3-cubic.

2.2. Characterization of catalysts

XRD patterns were obtained on a Bruker D8 (Bruker-AXS, Karlsruhe, Germany) diffractometer using a filtered Cu Kα radiation source (λ = 1.54178 Å), with accelerating voltage 40 kV, current 30 mA and scanned at 2θ from 10° to 70° with a rate of 0.02°/s. N_2 adsorption/desorption was measured using a Micromeritics Tristar 3000 to obtain pore volume and the Brunauer–Emmett–Teller (BET) specific surface area. Prior to measurement, samples were degassed at 120 °C for 5 h under vacuum condition. The BET surface area was calculated from adsorption at relative pressure of 0.05–0.15 using the BET equation and pore volume was determined from the adsorption at relative pressure of 0.99. The pore size distribution was obtained from desorption part using the BJH method. The external morphology and chemical compositions of the samples were observed on a ZEISS NEON 40EsB scanning electron microscope (SEM) equipped with an energy dispersive spectrometer (SEM-EDS).

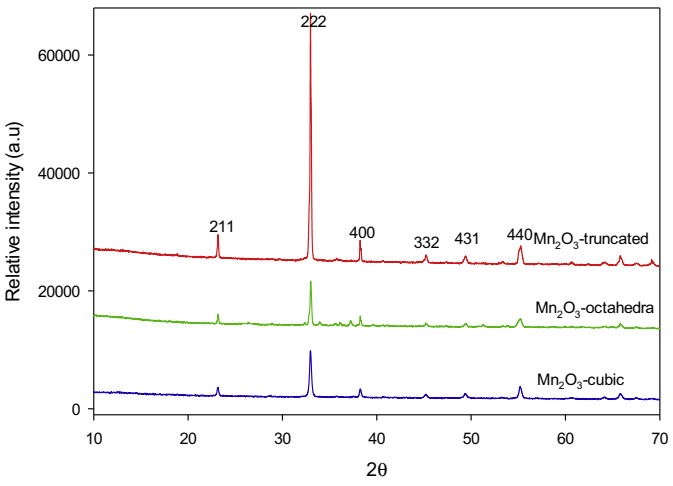

Fig. 1. XRD patterns of Mn_2O_3 catalysts.

2.3. Kinetic study of phenol oxidation

Phenol degradation tests were carried out in a 1-L glass beaker with 500 mL containing 25, 50, 75 and 100 mg/L of phenolic solutions. The reaction mixture was stirred constantly at 400 rpm. Firstly, a fixed amount of peroxymonosulfate (Oxone®, DuPont's triple salt: $2KHSO_5{\cdot}KHSO_4{\cdot}K_2SO_4$, Sigma–Aldrich) was added into the solution for a while, then a catalyst was added into the solution to start the oxidation reaction of phenol. At certain time, 0.5 mL of water sample was withdrawn from the mixture using a syringe filter of 0.45 μm and then mixed with 0.5 mL of pure methanol to quench the reaction. The concentration of phenol was analyzed using a Varian HPLC with a UV detector at λ = 270 nm. The column used was C-18 with mobile phase of 30% CH_3CN and 70% ultrapure water. For selected samples, total organic carbon (TOC) was determined using a Shimadzu TOC-5000 CE analyzer. For the recycle tests of the catalyst, after each run, the catalyst was obtained by filtration and thoroughly washed with distilled water several times, then dried at 80 °C for 2 h.

3. Results and discussion

Fig. 1 shows XRD patterns of three Mn-based catalysts. Three catalysts displayed similar XRD patterns, which are corresponding to the cubic structure of α-Mn_2O_3. No characteristic peaks due to other impurities were observed, suggesting the high purity of the samples.

SEM images of three samples are presented in Fig. 2. As can be seen, the samples present clearly in different morphologies. One from hydrothermal synthesis presented as a cubic single crystal with particle size of about 1–2 μm. The other two samples displayed in octahedral and truncated octahedral forms, which exhibited both aggregates and single crystal. For single crystal, the particle size is about 1–2 μm. The observations are similar to the samples reported in reference [23].

Fig. 3 shows N_2 adsorption isotherms and pore size distributions of three α-Mn_2O_3 samples in different shapes. The surface areas and

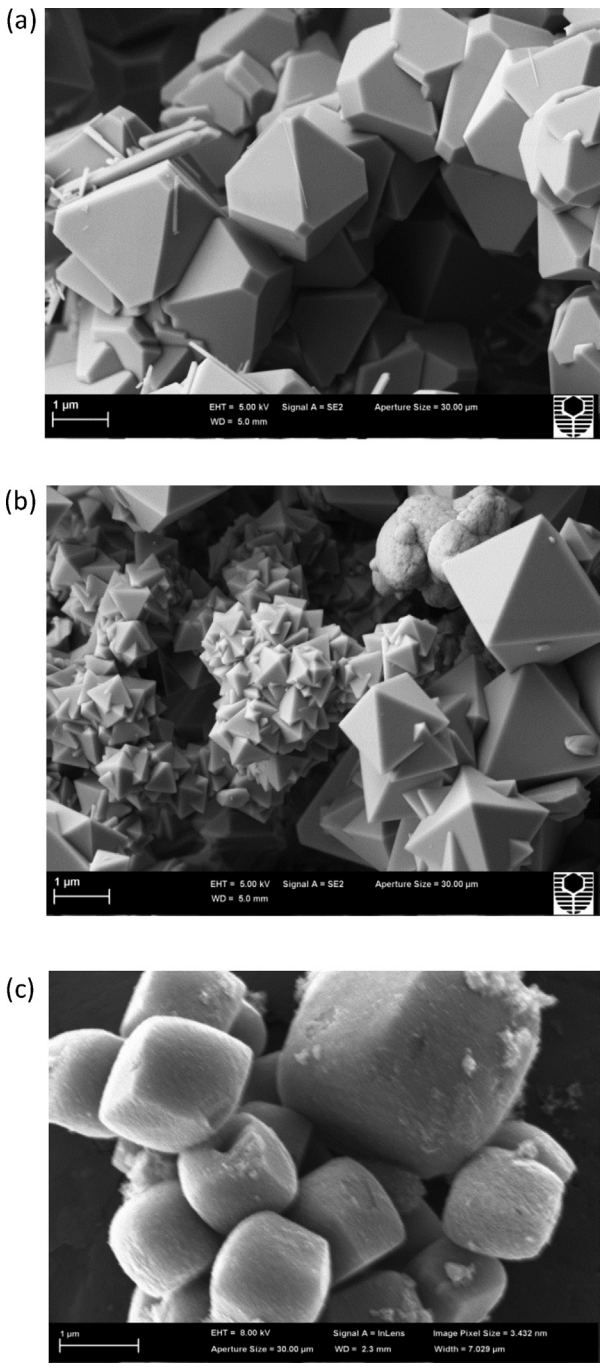

Fig. 2. SEM images of α-Mn_2O_3 catalysts. (a) α-Mn_2O_3-truncated octahedra, (b) α-Mn_2O_3-octahedra and (c) α-Mn_2O_3-cubic.

pore volumes are given in Table 1. Generally, α-Mn_2O_3-cubic presented higher N_2 adsorption than the other two α-Mn_2O_3 samples. The surface area and pore volume are 24 m^2/g and 0.17 $cm^3\ g^{-1}$, respectively. α-Mn_2O_3-octahedra and α-Mn_2O_3-truncated showed similar N_2 adsorption with low capacity, demonstrating non-porous structure. The surface areas for the both catalysts are lower than 5 m^2/g, however, α-Mn_2O_3-truncated showed slightly high surface area. The low surface areas of the three Mn_2O_3 samples suggest that they are less-developed porous and nonporous materials. SEM photos also show that the samples are composed of solid single crystals and aggregates, which results in much less surface area and pore volume. The surface area and pore volume from N_2 adsorption are mainly attributed to interparticle pores, which are usually in the range of mesopores. The slight difference in adsorption and desorption curves at low relative pressures ($p/p^0 \sim 0.2$) for α-Mn_2O_3-octahedra and α-Mn_2O_3-truncated is due to their nonporous structure and measurement errors. The pore size distributions of three α-Mn_2O_3 samples showed that α-Mn_2O_3-cubic has micropores in a range of 0.8–1.5 nm with a peak at 1.1 nm. α-Mn_2O_3-octahedra has more micropores at less than 1.5 nm while α-Mn_2O_3-truncated showed micropores at a peak of 1.3 nm.

The adsorption and degradation profiles of phenol against time on various α-Mn_2O_3 materials are shown in Fig. 4. α-Mn_2O_3-cubic showed somewhat initial adsorption of phenol and the adsorption arrived at equilibrium at 60 min with about 10% phenol removal. Other two α-Mn_2O_3 presented little phenol adsorption less than 5%. Previous investigations have demonstrated that Oxone® alone could not induce strong phenol degradation with less than 5% phenol removal [10,11]. However, α-Mn_2O_3 could activate Oxone® to induce strong phenol degradation. Three α-Mn_2O_3 samples presented different phenol degradation profiles. α-Mn_2O_3-truncated presented the least phenol degradation rate and phenol removal is about 50% at 180 min. α-Mn_2O_3-octahedra showed higher activity than α-Mn_2O_3-truncated with 100% phenol removal at 180 min. α-Mn_2O_3-cubic produced the highest phenol degradation rate and achieved 100% phenol removal in 60 min. Meanwhile for the TOC removal, α-Mn_2O_3-cubic produced 90% TOC removal while α-Mn_2O_3-truncated and α-Mn_2O_3-octahedra could only have 43% and 76% TOC removal, respectively (Table 1). These results suggest the order of catalytic activity of three α-Mn_2O_3 samples as α-Mn_2O_3-cubic > α-Mn_2O_3-octahedra > α-Mn_2O_3-truncated.

Based on the phenol degradation profiles, a first order kinetic model (Eq. (1)) was used for curve fitting.

$$\ln\left(\frac{C}{C_0}\right) = -k \cdot t \quad (1)$$

where k is the apparent first order rate constant of phenol removal, C is the concentration of phenol at various time (t). C_0 is the initial phenol concentration.

The results showed that the phenol degradation followed the first order kinetics and the rate constants for three α-Mn_2O_3 catalysts are given in Table 1. α-Mn_2O_3-cubic showed the reaction rate at 15 times higher than that α-Mn_2O_3-truncated. Previous investigations have showed that phenol degradation on Co and Mn-based catalyst follows first order kinetics [9,25–28].

In this investigation, three different shaped α-Mn_2O_3 crystals showed different activities in activation of Oxone® for phenol degradation, which can be related to the variations in textural and crystalline structure and other physicochemical properties. Generally, the catalytic activity is related to the surface area of solid catalysts. BET measurements showed that α-Mn_2O_3-cubic has the highest surface area and as a result it shows some phenol adsorption. α-Mn_2O_3-octahedra and α-Mn_2O_3-truncated have lower surface areas less than 5 m^2/g, while α-Mn_2O_3-truncated

Table 1
Properties of various α-Mn_2O_3 samples and their catalytic activity in phenol degradation.

Catalyst	Structure	S_{BET} (m^2/g)	Pore volume (V, $cm^3\ g^{-1}$)	Rate constant (min^{-1})	TOC reduction (%)
α-Mn_2O_3-truncated	Bixbyte-C	4.0	0.011	0.0042	43.2
α-Mn_2O_3-octahedra	Bixbyte-C	1.1	0.002	0.0091	76.4
α-Mn_2O_3-cubic	Bixbyte-C	24.2	0.166	0.0615	90.5

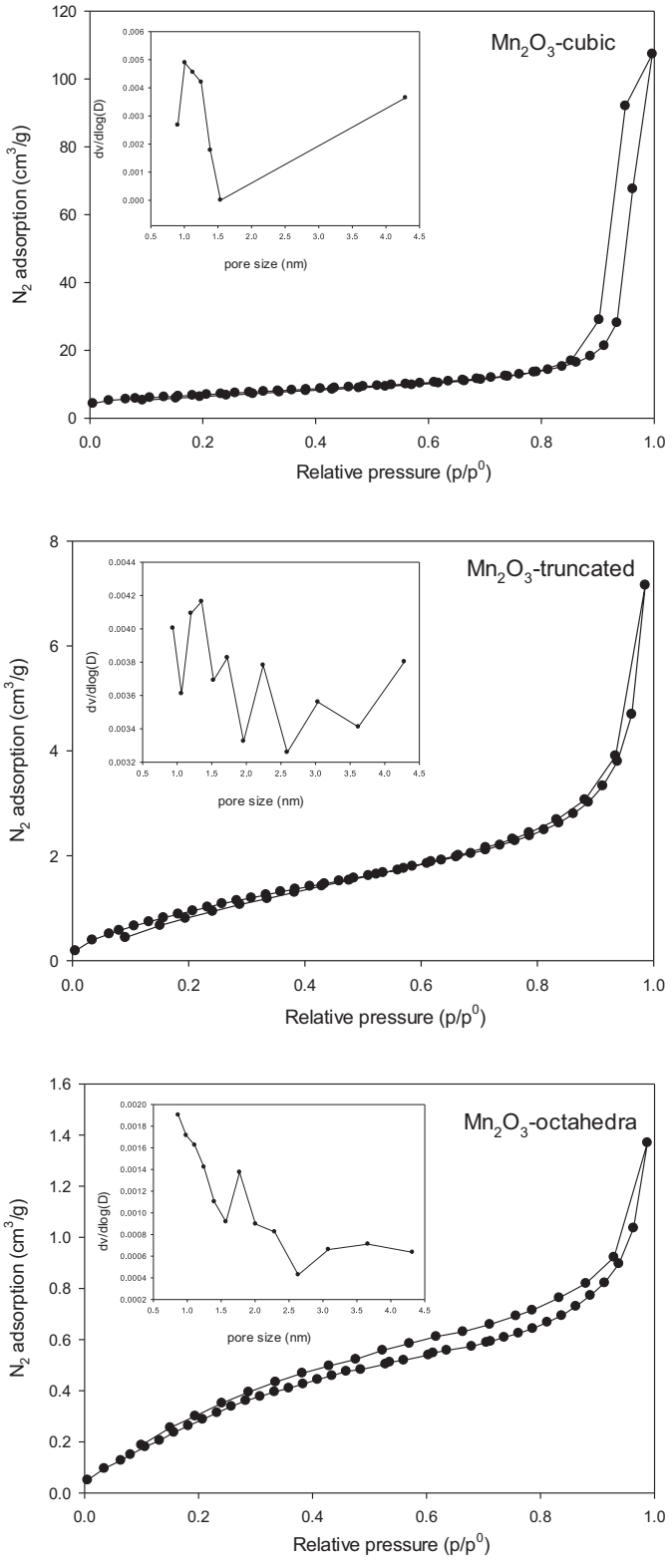

Fig. 3. N_2 adsorption–desorption isotherms and pore size distributions of Mn_2O_3 catalysts.

shows higher surface area than α-Mn_2O_3-octahedra. Cao et al. [29] have synthesized various Mn_2O_3 hollow structures, such as spheres, cubes, ellipsoids, and dumbbells, and tested them in phenol adsorption. They found that BET surface areas of hollow Mn_2O_3 spheres, cubes, ellipsoids, and dumbbells are 15, 20, 24, and 19 m^2/g, respectively, and that they could respectively remove

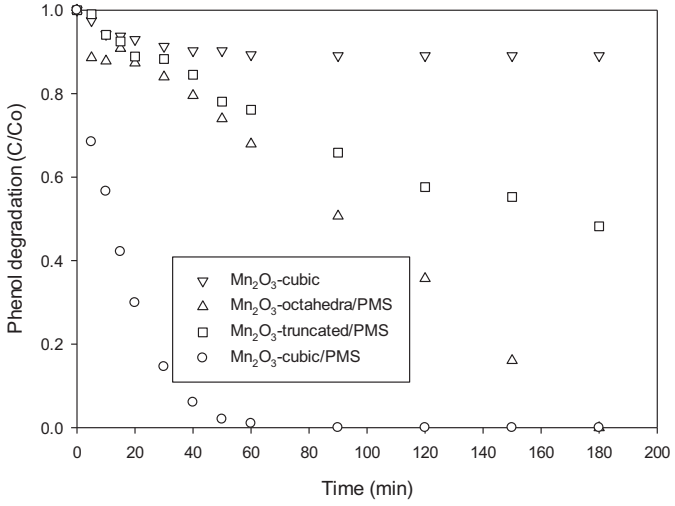

Fig. 4. Phenol reduction with time in adsorption and catalytic oxidation. Reaction conditions: [phenol] = 25 ppm, catalyst = 0.4 g/L, oxone = 2 g/L, and T = 25 °C.

about 77%, 83%, 81%, and 78% of phenol at the testing conditions. Their results suggest that the adsorption is closely related to surface area and that high surface area will result in good adsorption. However, in further comparison with the catalytic activity of the three Mn_2O_3 samples in the investigation, it was seen that the catalytic performance cannot be significantly influenced by the surface areas. For the pore size, though three Mn_2O_3 samples showed some similar micropores, α-Mn_2O_3-octahedra and α-Mn_2O_3-truncated presented practically nonporous structure. Thus, pore size will not be an important factor influencing Mn_2O_3 catalytic activity.

For shape selective catalysis of manganese oxides, Li et al. [21] investigated shape effect of Mn_3O_4 in photocatalysis of Rhodamine B and found that the photodecomposition activity of Mn_3O_4 nano-octahedra is much superior to that of commercial Mn_3O_4 powders. Fei et al. [19] prepared Mn_3O_4 nanocrystallites with three distinct morphologies (cubic, hexagonal, and octahedral) and evaluated their activities for benzene combustion. Three catalysts showed the catalytic activity in an order of hexagonal > cubic > octahedral. The dominant exposed facets for the three kinds of Mn_3O_4 polyhedrons show the activity order: (1 0 3) > (2 0 0) > (1 0 1).

Li et al. [23] investigated shape evolution of Mn_2O_3 formation and concluded that formation of Mn_2O_3 evolves from nanocubes, then cuboctahedra, and finally octahedra due to the different growth rate of (0 0 1) and (1 1 1) faces (Scheme 1). The catalytic activity in pyridoin conversion to quinoxaline showed that octahedral Mn_2O_3 exhibited higher conversion than truncated-octahedral Mn_2O_3.

In this work, catalytic degradation of phenol on Mn_2O_3 is different on varying shapes of Mn_2O_3 crystal, also demonstrating the shape effect as reported in the above investigations. The order of catalytic activity is α-Mn_2O_3-cubic > α-Mn_2O_3-octahedra > α-Mn_2O_3-truncated, which is not the order of BET surface areas. The

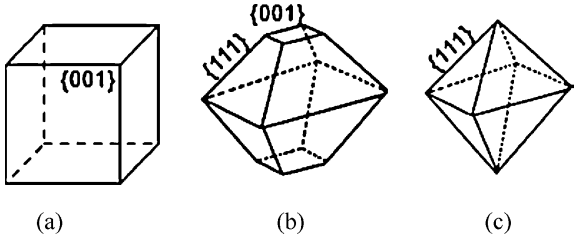

Scheme 1. Crystalline facets of different shaped Mn_2O_3 crystals. (a) Cube, (b) truncated octahedra and (c) octahedra [23].

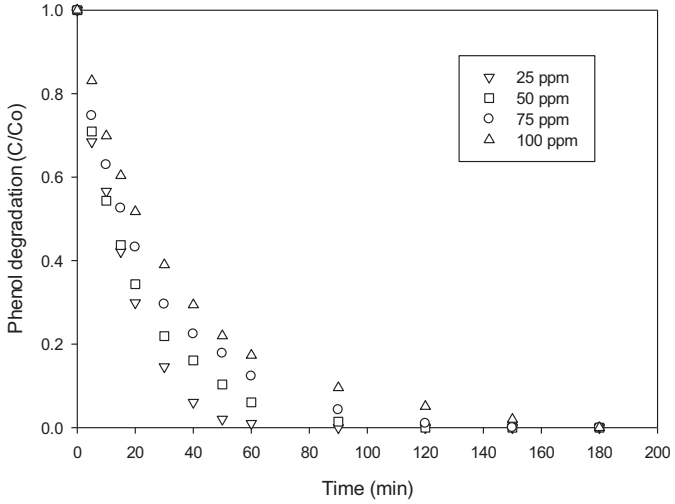

Fig. 5. Effect of phenol concentration on phenol removal. Reaction conditions: catalyst = 0.4 g/L, oxone = 2 g/L, and T = 25 °C.

catalytic activity therefore can be related to the surface facet activity. The evolution of the facets in Mn_2O_3 synthesis has suggested the activity as cube > octahedra. Therefore, it is deduced that the high phenol degradation of α-Mn_2O_3-cubic is attributed to its high surface area, phenol adsorption and active surface facet with the inherent distinction of surface atoms arrangement.

Further investigations were conducted to understand the effect of reaction conditions on phenol degradation using the most effective catalyst, α-Mn_2O_3-cubic. Fig. 5 presents phenol degradation efficiencies at varying initial phenol concentrations. With increased phenol concentration, phenol removal efficiency would decrease. At phenol concentration of 75 or 100 mg/L, complete degradation would take 120 and 180 min, respectively. The observation is similar to other investigations [10,11,25].

Fig. 6 shows phenol degradation profiles on α-Mn_2O_3-cubic at varying temperatures. In general, higher temperature will enhance the reaction rate of phenol degradation and efficiency of phenol removal can reach 100% at 20 min at 45 °C. From the first order kinetics, reaction rate constants were determined from all the degradation profiles and the correlation between the rate constant and temperature was fitted by the Arrhenius relationship as shown

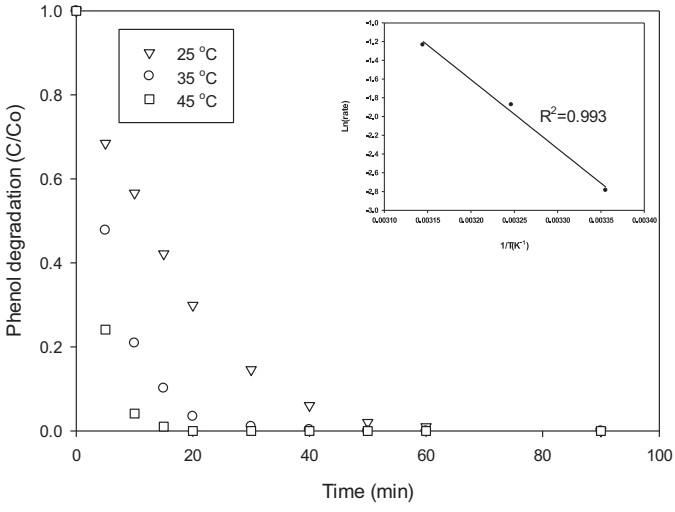

Fig. 6. Effect of temperature on phenol removal. Reaction conditions: [phenol] = 25 ppm, catalyst = 0.4 g/L, and oxone = 2 g/L.

Table 2
A comparison of activation energy of Mn-based catalysts.

Catalyst	Organics	Activation energy (kJ/mol)	Reference
Mn_3O_4–rGO	Orange II	49.5	[30]
α-MnO_2 wire	Phenol	21.9	[12]
Mn_2O_3 sphere	Phenol	11.4	[31]
Mn_2O_3 cube	Phenol	61.2	This investigation

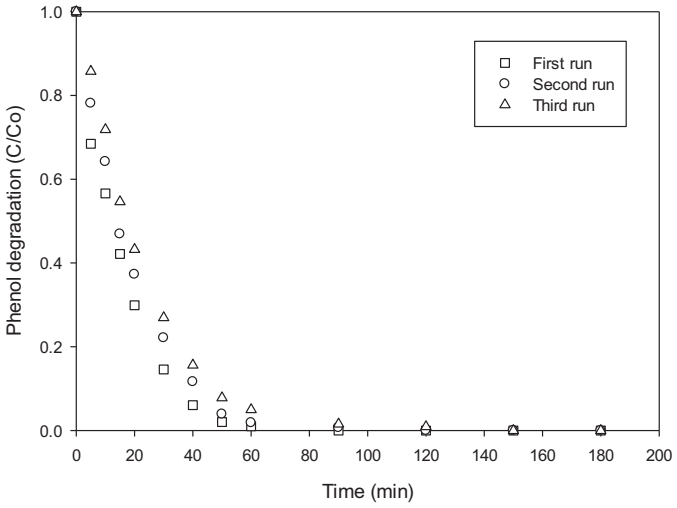

Fig. 7. Degradation of phenol in multiple uses of Mn_2O_3-cubic like catalyst. Reaction conditions: [phenol] = 25 ppm, catalyst = 0.4 g/L, and oxone = 2 g/L.

in the inset of Fig. 6. The activation energy was thus calculated to be 61.2 kJ/mol.

In the past few years, several Mn-based catalysts have been tested in activation of Oxone® for aqueous organic oxidation. Table 2 shows the activation energies obtained from the investigations. As seen, Mn_2O_3 cube presents higher activation energy than other Mn-based catalysts.

Fig. 7 shows the activity of regenerated α-Mn_2O_3-cubic by simple water washing in phenol degradation. One can see that α-Mn_2O_3-cubic presented slightly decreased activity in second and third runs. Phenol degradation efficiency could also be 100% in 90 min, suggesting high stability of α-Mn_2O_3-cubic and its reusability. Slight decrease in reaction rate is attributed to the adsorption of intermediates on the surface of α-Mn_2O_3-cubic. The intermediates could not be completely removed by simple water washing but could be removed by calcination [32].

4. Conclusions

Several single crystals of α-Mn_2O_3 catalysts with cubic, octahedral and truncated-octahedral forms were prepared and their shape-control activity was evaluated in catalytic activation of Oxone® for phenol degradation. Cubic α-Mn_2O_3 presented a higher surface area and a more active surface facet than those of octahedral and truncated octahedral α-Mn_2O_3. Catalytic evaluation in phenol degradation showed that cubic α-Mn_2O_3 presented the highest catalytic activity. Catalytic degradation of phenol was also influenced by reaction conditions, initial phenol concentration and temperature. Kinetic studies showed that phenol degradation could be described by a first-order kinetic model and the activation energy is 61.2 kJ/mol. Cubic α-Mn_2O_3 also exhibited high catalytic stability with little deactivation after several tests.

References

[1] R.B. Jackson, S.R. Carpenter, C.N. Dahm, D.M. McKnight, R.J. Naiman, S.L. Postel, S.W. Running, Ecological Applications 11 (2001) 1027–1045.
[2] S. Wang, Dyes and Pigments 76 (2008) 714–720.
[3] E.A. Betterton, M.R. Hoffmann, Environmental Science & Technology 24 (1990) 1819–1824.
[4] G.P. Anipsitakis, D.D. Dionysiou, Environmental Science & Technology 38 (2004) 3705–3712.
[5] S.K. Ling, S. Wang, Y. Peng, Journal of Hazardous Materials 178 (2010) 385–389.
[6] X. Chen, X. Qiao, D. Wang, J. Lin, J. Chen, Chemosphere 67 (2007) 802–808.
[7] Y.R. Wang, W. Chu, Journal of Hazardous Materials 186 (2011) 1455–1461.
[8] H. Sun, G. Zhou, S. Liu, H.M. Ang, M.O. Tade, S. Wang, ACS Applied Materials & Interfaces 4 (2012) 6235–6241.
[9] Y. Yao, Z. Yang, D. Zhang, W. Peng, H. Sun, S. Wang, Industrial & Engineering Chemistry Research 51 (2012) 6044–6051.
[10] E. Saputra, S. Muhammad, H. Sun, H.-M. Ang, M.O. Tade, S. Wang, Journal of Colloid and Interface Science 407 (2013) 467–473.
[11] E. Saputra, S. Muhammad, H. Sun, A. Patel, P. Shukla, Z.H. Zhu, S. Wang, Catalysis Communications 26 (2012) 144–148.
[12] E. Saputra, S. Muhammad, H. Sun, H.M. Ang, M.O. Tade, S. Wang, Environmental Science & Technology 47 (2013) 5882–5887.
[13] E. Saputra, S. Muhammad, H. Sun, H.-M. Ang, M.O. Tadé, S. Wang, Applied Catalysis B: Environmental 142–143 (2013) 729–735.
[14] K. Lee, M. Kim, H. Kim, Journal of Materials Chemistry 20 (2010) 3791–3798.
[15] Z. Quan, Y. Wang, J. Fang, Accounts of Chemical Research 46 (2013) 191–202.
[16] C.Z. Wen, H.B. Jiang, S.Z. Qiao, H.G. Yang, G.Q. Lu, Journal of Materials Chemistry 21 (2011) 7052–7061.
[17] Z.-Y. Zhou, N. Tian, J.-T. Li, I. Broadwell, S.-G. Sun, Chemical Society Reviews 40 (2011) 4167–4185.
[18] H. Sun, H.M. Ang, M.O. Tade, S. Wang, Journal of Materials Chemistry A 1 (2013) 14427–14442.
[19] Z.-Y. Fei, B. Sun, L. Zhao, W.-J. Ji, C.-T. Au, Chemistry – A European Journal 19 (2013) 6480–6487.
[20] H. Li, G. Qi, Tana, X. Zhang, W. Li, W. Shen, Catalysis Science & Technology 1 (2011) 1677–1682.
[21] Y. Li, H. Tan, X.-Y. Yang, B. Goris, J. Verbeeck, S. Bals, P. Colson, R. Cloots, G. Van Tendeloo, B.-L. Su, Small 7 (2011) 475–483.
[22] W. Xiao, D. Wang, X.W. Lou, Journal of Physical Chemistry C 114 (2010) 1694–1700.
[23] W.-N. Li, L. Zhang, S. Sithambaram, J. Yuan, X.-F. Shen, M. Aindow, S.L. Suib, Journal of Physical Chemistry C 111 (2007) 14694–14697.
[24] S. Lei, K. Tang, Z. Fang, Q. Liu, H. Zheng, Materials Letters 60 (2006) 53–56.
[25] P.R. Shukla, S. Wang, H. Sun, H.M. Ang, M. Tade, Applied Catalysis B – Environmental 100 (2010) 529–534.
[26] H. Liang, H. Sun, A. Patel, P. Shukla, Z.H. Zhu, S. Wang, Applied Catalysis B – Environmental 127 (2012) 330–335.
[27] E. Saputra, S. Muhammad, H. Sun, H.M. Ang, M.O. Tade, S. Wang, Catalysis Today 190 (2012) 68–72.
[28] Y. Yao, Z. Yang, H. Sun, S. Wang, Industrial & Engineering Chemistry Research 51 (2012) 14958–14965.
[29] J. Cao, Y. Zhu, K. Bao, L. Shi, S. Liu, Y. Qian, Journal of Physical Chemistry C 113 (2009) 17755–17760.
[30] Y. Yao, C. Xu, S. Yu, D. Zhang, S. Wang, Industrial & Engineering Chemistry Research 52 (2013) 3637–3645.
[31] E. Saputra, S. Muhammad, H. Sun, H.-M. Ang, M.O. Tade, S. Wang, Applied Catalysis B – Environmental 142 (2013) 729–735.
[32] H. Sun, H. Liang, G. Zhou, S. Wang, Journal of Colloid and Interface Science 394 (2013) 394–400.